Optics Letters

All-fiber frequency comb at 2 μm providing 1.4-cycle pulses

Sida Xing,[1,2,*] Abijith S. Kowligy,[1,2] Daniel M. B. Lesko,[1,2] Alexander J. Lind,[1,2] and Scott A. Diddams[1,2]

[1]Time and Frequency Division, NIST, 325 Broadway, Boulder, Colorado 80305, USA
[2]Department of Physics, University of Colorado, 2000 Colorado Ave., Boulder, Colorado 80309, USA
*Corresponding author: sida.xing@colorado.edu

Received 26 February 2020; revised 30 March 2020; accepted 31 March 2020; posted 3 April 2020 (Doc. ID 391486); published 1 May 2020

We report an all-fiber approach to generating sub-2-cycle pulses at 2 μm and a corresponding octave-spanning optical frequency comb. Our configuration leverages mature erbium:fiber laser technology at 1.5 μm to provide a seed pulse for a thulium-doped fiber amplifier that outputs 330 mW average power at a 100 MHz repetition rate. Following amplification, nonlinear self-compression in fiber decreases the pulse duration to 9.5 fs, or 1.4 optical cycles. The spectrum of the ultrashort pulse spans from 1 to beyond 2.4 μm and enables direct measurement of the carrier-envelope offset frequency. Our approach employs only commercially available fiber components, resulting in a design that is easy to reproduce in the larger community. As such, this system should be useful as a robust frequency comb source in the near-infrared or as a pump source to generate mid-infrared frequency combs.

https://doi.org/10.1364/OL.391486

Compact, coherent, and broad bandwidth laser frequency comb sources in the mid-infrared (MIR) region (3 to 25 μm) are essential components for molecular spectroscopy, environmental monitoring, and other applications [1–3]. While a few frequency comb lasers directly emit in the MIR [4–7], nonlinear frequency conversion from the near-infrared is a general and reliable way to coherently convert mature near-infrared frequency comb sources to MIR wavelengths [8–16]. Among different pump lasers for nonlinear conversion, the 2 μm band with thulium (Tm)-doped silica fiber holds some unique advantages. The lower photon energy of 2 μm light expands the possibility of nonlinear materials due to reduced multi-photon absorption, and leads to efficient and high power intra-pulse different frequency generation (IP-DFG) [11,17]. Additionally, for efficient MIR supercontinuum generation (SCG) in waveguides, the longer pump wavelength also requires less dispersion engineering than telecom band pumps [12]. In addition, frequency comb sources near 2 μm are promising for high precision and sensitive spectroscopy. CO, CO_2, NH_3, and CH_4 have absorption peaks in the 2 μm band [18,19], and direct use of 2 μm light has already attracted interest from the spectroscopy community [20,21]. Finally, the 2 μm wavelength resides in the high transmission window of silica fibers, leading to good availability of commercial components and the same fiber processing techniques as the telecom fibers.

For the generation of ultrashort pulses at 2 μm with Tm-doped fibers (TDFs), fiber-based chirped-pulse-amplification (CPA) can deliver multi-watt output [10,22–24], but it remains challenging to broaden and compress such pulses to the few-cycle region. Compression with free-space gratings has been limited to an 80 fs range [22,23] due to the 3rd-order dispersion and insufficient pulse broadening. To achieve a broadband spectrum, it is essential to perform SCG in a well-controlled manner. In this arena, two main methods are available to yield isolated pulses with octave-spanning spectra: nonlinear self-compression [25] and SCG in normal dispersion fibers [26]. The nonlinear self-compression method combines spectral broadening and compression in one single fiber, making it ideal for implementation in an all-fiber setup. As early as 2007 [25], researchers demonstrated nonlinear self-compression of 2 μm pulses to 17 fs, 0.27 mJ in gas filament. Only very recently [17], 13 fs, 90 nJ pulses were successfully generated using a photonic crystal fiber at 2 μm band.

In this Letter, to the best of our knowledge, we present the first sub-2-cycle (9.5 fs) frequency comb source implemented using an all-fiber configuration at 2 μm. By soliton self-frequency shift in highly nonlinear fiber (HNLF), the seed laser converts the commercially available low noise 1.56 μm frequency comb to 2 μm. A fiber CPA amplifies the 2 μm seed pulse to 420 mW. A two-stage self-compression scheme reduces the pulse duration to 9.5 fs and outputs 327 mW average power at a 100 MHz repetition rate. The experimental data show excellent agreement with our simulations in both spectral and temporal domains. With only 12 mW of the output power an inline $f-2f$ setup is used to recover a 30 dB signal-to-noise ratio (SNR) at a 300 kHz resolution bandwidth (RBW). The carrier-envelope offset (CEO) frequency, f_{ceo}, has a 3 dB bandwidth of approximately 5 kHz, indicating no degradation of the 1.5 μm seed source. Additionally, from the practical side, the whole seed, CPA, and compressor can easily fit on a 35 cm × 30 cm breadboard. We only used commercially available components

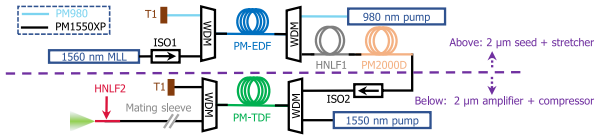

Fig. 1. Experimental setup of the Tm-doped fiber amplifier. MLL, mode-locked laser; ISO, isolator; WDM, wavelength-division multiplexer; T1, terminated port; PM-EDF, polarization-maintaining erbium-doped fiber; HNLF, highly nonlinear fiber; PM-TDF, polarization-maintaining thulium-doped fiber.

in our implementation, making the laser easily repeatable and accessible.

Figure 1 shows the all-PM fiber configuration for producing 2 μm ultrashort pulses. We begin with 20 mW average power at a 100 MHz repetition rate from a Menlo Systems Figure-9 mode-locked laser that is amplified to 190 mW using a backward pumped nLight PM erbium (Er)-doped fiber and a 1 W PM 980 nm pump diode. After amplification and self-compression, the pulse before HNLF1 is measured to be 50 fs using a frequency resolved optical gating (FROG). The amplified light is then sent into a 30 cm PM HNLF1 (OFS Optics) to generate a 2 μm pulse by a Raman soliton self-frequency shift [6,24,27]. The HNLF 1 group velocity dispersion (GVD, β_2) is $-7.82\ \mathrm{ps}^2/\mathrm{km}$, and the nonlinear parameter (γ) is $10\ (\mathrm{W{-}km})^{-1}$ at 1550 nm. The soliton is centered at 1928 nm with a 100 nm bandwidth, 45 fs pulse duration, and average power of 40 mW. We then use 3 m of Nufern PM2000D to stretch the soliton and ensure net normal dispersion inside the CPA. We estimated the dispersion of PM2000D using [28] to be $92\ \mathrm{ps}^2/\mathrm{km}$. The stretched pulse then passes a fast-axis blocked PM-isolator (ISO2) with 0.8 dB insertion loss. The isolator blocks backward amplified spontaneous emission and filters the light on the fast-axis, and the polarization extinction ratio (PER) following ISO2 is measured to be greater than 20 dB. A PM-WDM, with <1 dB insertion loss from 1840 to 2100 nm, combines the 2 μm seed and continuous-wave 1550 nm pump light. This provides close to 30 mW of the 2 μm seed for the PM-TDF, which consists of 2 m of Nufern PM-TSF-9/125 fiber. The forward pumping scheme favors amplification in the 1900 nm region, and the output PM-WDM has >20 dB isolation between 1.55 and 2 μm to efficiently remove the residual C-band pump. The output of the amplifier connects to the compression fiber through a narrow-key FC/APC mating sleeve for flexibility in optimizing the compression stages, but it could be spliced instead.

For efficient pulse compression, we utilized a two-stage compression scheme. In the first stage, Nufern PM1550XP fiber compensates for the net normal dispersion of the CPA. The optimal fiber length is found to be 64 cm from a cutback test. After the first nonlinear compression stage, the pulse duration is near transform-limited at about 90 fs. The second compression stage utilizes nonlinear self-compression inside an elliptical core PM-HNLF from OFS (HNLF2 in Fig. 1). The HNLF2 is spliced to the PM1550XP using a CO_2 laser splicer, with combined splicing and Fresnel reflection losses of 1.2 dB. The strength of the nonlinear compression depends on the power from the thulium amplifier. At the shortest pulse duration, the 2 μm output power is 327 mW with a 1550 nm pump power of 1.94 W, yielding close to 17% efficiency. Since thulium has more efficient pump absorption at 1.6 μm [29], we expect higher pump efficiency if a 1.6 μm pump is used. After HNLF2, the output is collimated using an off-axis parabolic (OAP) mirror for pulse characterization and other applications. Using a broadband (1000 nm to 2000 nm) polarizer, the compressed pulse PER is measured to be more than 15 dB.

Two optical spectrum analyzers (OSA) were used to record the complete spectrum. A Yokogawa AQ6375 recorded spectra in the region of 1200 to 2400 nm, and when the laser output power was above 270 mW, the spectrum below 1200 nm was recorded using a Yokogawa AQ 6370. The solid lines in Fig. 2 show the recorded spectra at four output powers ranging from 145 to 327 mW. The amplifier output power from 145 to 330 mW corresponds to 0.7 to 1.94 W pump power. Empirically [10,30–32], a structured central region of the spectrum with smooth wings covering about one octave is a general indication of successful self-compression. A more detailed study of pulse quality, duration, and temporal distribution requires use of a generalized nonlinear Schrodinger equation (GNLSE) with the inclusion of Raman term, shock term and 7th-order dispersion. Numerically, implementing the GNLSE from [33], we simulated the complete process from the 2 μm seed soliton to the self-compressed output. The HNLF2 GVD is about $-13\ \mathrm{ps}^2/\mathrm{km}$, and the nonlinear parameter is $3.1\ (\mathrm{W{-}km})^{-1}$ at 1930 nm. The fiber parameters used in the simulation are the same for all output power levels (Fig. 2). Due to the short length of HNLF2 (6 cm), the linear propagation loss in silica fiber can be safely ignored, even for the 2.5 μm part of the spectrum [34].

The optimal 6 cm length of HNLF2 to produce the shortest pulse is influenced by both the TDF gain center and the self-compression length. The TDF gain center moves to a shorter wavelength with increased C-band pump power. For the best SNR, it is beneficial to set the CPA output spectrum peak to overlap with the seed pulse peak. In this case, we found that the optimal C-band pump power is around 1.9 W, which gave an output power of 327 mW. Figure 3 shows the simulated pulse evolution along HNLF2 under these conditions, with the simulated output pulse from first stage compression being used as the input pulse for the simulation. The pulse evolution of Fig. 3 indicates that most of the pulse broadening happens within the last 1 cm propagation of HNLF2, with the maximum at about 6 cm. In Fig. 3(b), we show the corresponding temporal evolution of the pulse. At the end of HNLF2, the simulated pulse duration is 9.2 fs, with a portion of the laser output power going into satellite pulses. From the simulation, we estimate that

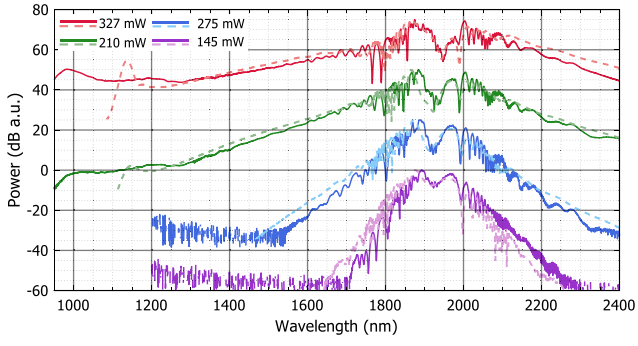

Fig. 2. Simulated spectra (dashed lines) and measured spectra (solid lines) for different powers. For better illustration, each spectrum is shifted by 25 dB. All the simulations share the same fiber parameters.

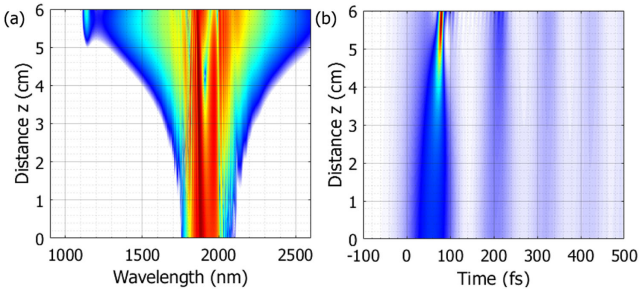

Fig. 3. Simulation of pulse propagation in HNLF2. (a) Spectral evolution along the fiber length (color in log scale); (b) corresponding temporal evolution along fiber length (color in linear scale).

the main peak contains 35% of the total power, leading to a peak power of 110 kW.

We characterize the pulses with second-harmonic generation FROG (SHG-FROG). In Figs. 4(a) and 4(b), we show the recorded and reconstructed FROG spectrograms. The FROG scan range is ±600 fs, and the reconstructed spectrogram has an error of 1.1 %. In Fig. 4(c), we zoom in at ±300 fs where we see excellent agreement between the simulated pulse duration of 9.2 fs and the reconstructed pulse of 9.5 fs. We check for satellite pulses by increasing the range to ±1.2 ps, but find no signal beyond −200 fs. Thus, the inset of Fig. 4(c) shows, the range from −200 to 1200 fs, where the simulation still matches well with the experiment. Using the data from a ±1.2 ps scan range, the main peak contains about 32 % of total power, hence 104 kW in the peak, with 10 % loss due to Fresnel reflection at the end of HNLF2. We measured the pulse duration at various laser powers [dots in Fig. 4(d)]. Just as the simulation matches the measured spectra for various laser powers (Fig. 2), the retrieved pulse duration matches the simulation at all laser powers. In Fig. 4(e), we show the simulated pulse duration as a function of HNLF2 length. To generate around 9.5 fs pulses, we can tolerate a ± 2 mm error on the fiber length, which is achieved using a normal ruler.

With an octave-spanning spectrum available from the soliton self-compression, it is possible to retrieve the f_{ceo} in a straightforward manner [35]. For a high SNR on f_{ceo}, the second harmonic (SH) and DW should have good temporal overlap. The pulse evolution simulation in Fig. 3(a) indicates the 1 μm DW builds a moderate power at about 5.8 cm, and there is small walk-off in less than 2 mm of propagation. In addition, the SHG of the 2 μm pulse falls right on the DW pulse peak. Therefore, we expect to have an f_{ceo} with a high SNR by directly beating the SH of the 2 μm pulse with the DW, using no extra pulse delay control.

The experimental setup for f_{ceo} measurement is drawn in Fig. 5(a). To use the minimum power for f_{ceo} detection, a partially reflective metallic neutral-density filter (Thorlabs continuous variable NDC-100C-4M filter) is used to separate 3.5% (13 mW) of the few-cycle pulse, which is focused into a 1 mm PPLN with a poling period of 30 μm. An angle-tuned bandpass (BP) filter at (1075 ± 25) nm passes the DW and SHG light onto the detector (EOT-3000 A), and the f_{ceo} heterodyne spectrum is recorded on an electrical spectrum analyzer. At 300 kHz RBW, >30 dB SNR is seen Fig. 5(b). Figure 5(c) shows the f_{ceo} spectrum at 1 kHz RBW with 3 dB bandwidth of 5 kHz, which is consistent with the linewidth of the Er:fiber mode-locked laser (MLL). Such an SNR is high enough for a stable frequency comb locking. Meanwhile, about 96 % of CEO-stabilized light is available for other applications. We note that better f_{ceo} SNR

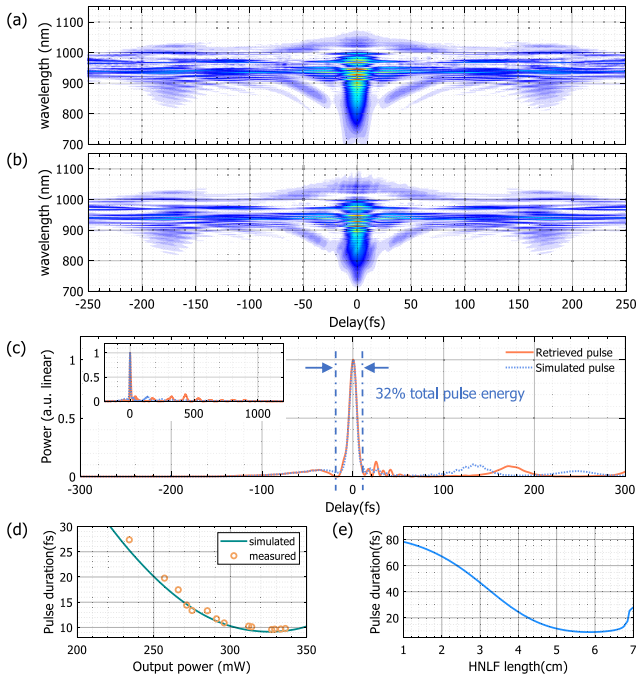

Fig. 4. (a) Experimental and (b) reconstructed SHG FROG spectrogram. (c) Retrieved (solid) and simulated pulse (dotted). Inset: retrieved pulse (solid line) and simulated pulse (dotted line) for a delay range is –200 fs to 1200 fs, respectively. (d) FROG retrieved pulse duration (dots) and simulated pulse duration (line) as a function of laser output power. (e) Simulated pulse duration as it propagates along the HNLF2.

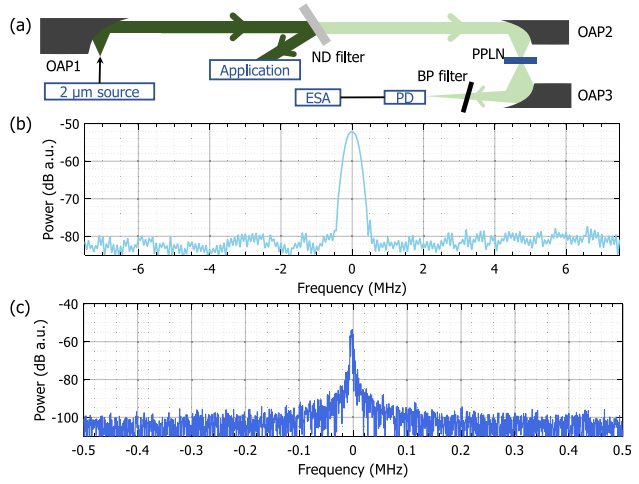

Fig. 5. (a) Experimental setup for f_{ceo} retrieval. A reflective neutral-density (ND) filter is a dispersion-free beam splitter for the reflected beam. The arrows are the beam propagation direction. PPLN: periodically poled lithium niobate. BP filter: bandpass filter. PD: photodiode. ESA: electrical spectrum analyzer. OAP: off-axis parabolic mirror. (b) f_{ceo} at 300 kHz RBW; a frequency offset of 57.5 MHz is applied. (c) f_{ceo} at 1 kHz RBW, with the same 57.5 MHz offset.

with even less power should be possible with a BP filter centered at 990 nm to utilize higher SHG and DW powers.

In summary, we demonstrated and characterized an all-fiber 2 μm frequency comb that outputs 9.5 fs (1.4-cycle) pulses. The average output power is 327 mW under a 1.94 W C-band pump. Improving the pulse quality from the first compression stage will contribute to higher power in the central pulse. An L-band EDFA with a larger doping concentration TDF can be a simple improvement. Our result represents the first sub-2-cycle 2 μm frequency comb in a compact, robust, and efficient all-fiber configuration. Importantly, the use of all commercially available components makes our laser repeatable and reliable, with stable "hands-free" operation from day to day. This setup is also scalable in repetition rate, leading to more energy in each comb line. For example, we anticipate an all-PM commercially available heavily doped Tm-fiber will lead to sub-2-cycle 2 μm lasers working at a gigahertz repetition rates [36]. At the same time, milliwatt-level peak powers at a 100 MHz repetition rate should be feasible with a photonic crystal fiber at the last compression stage. Finally, even shorter pulses could be feasible through coherent pulse superposition with other regions of the spectrum also generated from the 1.5 μm seed [37].

Funding. Air Force Office of Scientific Research (FA9550-16-1-0016); Physical Measurement Laboratory; Defense Advanced Research Projects Agency.

Acknowledgment. The mention of specific companies, products, or trade names does not constitute an endorsement by NIST. The authors thank E. Baumann and N. Nader for their comments and H. Timmers for his assistance.

Disclosures. The authors declare no conflicts of interest.

REFERENCES

1. N. Picqué and T. W. Hänsch, Nat. Photonics **13**, 146 (2019).
2. K. C. Cossel, E. M. Waxman, I. A. Finneran, G. A. Blake, J. Ye, and N. R. Newbury, J. Opt. Soc. Am. B **34**, 104 (2017).
3. M. Vainio and L. Halonen, Phys. Chem. Chem. Phys. **18**, 4266 (2016).
4. A. Hugi, G. Villares, S. Blaser, H. C. Liu, and J. Faist, Nature **492**, 229 (2012).
5. S. Duval, M. Bernier, V. Fortin, J. Genest, M. Piché, and R. Vallée, Optica **2**, 623 (2015).
6. A. Klose, G. Ycas, D. L. Maser, and S. A. Diddams, Opt. Express **22**, 28400 (2014).
7. S. Vasilyev, V. Smolski, J. Peppers, I. Moskalev, M. Mirov, Y. Barnakov, S. Mirov, and V. Gapontsev, Opt. Express **27**, 35079 (2019).
8. A. S. Kowligy, H. Timmers, A. J. Lind, U. Elu, F. C. Cruz, P. G. Schunemann, J. Biegert, and S. A. Diddams, Sci. Adv. **5**, eaaw8794 (2019).
9. C. Gaida, M. Gebhardt, T. Heuermann, F. Stutzki, C. Jauregui, J. Antonio-Lopez, A. Schülzgen, R. Amezcua-Correa, A. Tünnermann, I. Pupeza, and J. Limpert, Light Sci. Appl. **7**, 94 (2018).
10. T. P. Butler, N. Lilienfein, J. Xu, N. Nagl, C. Hofer, D. Gerz, K. F. Mak, C. Gaida, T. Heuermann, M. Gebhardt, J. Limpert, F. Krausz, and I. Pupeza, J. Phys. Photonics **1**, 44006 (2019).
11. J. Zhang, K. Fritsch, Q. Wang, F. Krausz, K. F. Mak, and O. Pronin, Opt. Lett. **44**, 2986 (2019).
12. N. Nader, A. Kowligy, J. Chiles, E. J. Stanton, H. Timmers, A. J. Lind, F. C. Cruz, D. M. B. Lesko, K. A. Briggman, S. W. Nam, S. A. Diddams, and R. P. Mirin, Optica **6**, 1269 (2019).
13. K. Liu, H. Liang, S. Qu, W. Li, X. Zou, Y. Zhang, and Q. J. Wang, Opt. Express **27**, 37706 (2019).
14. P. Krogen, H. Suchowski, H. Liang, N. Flemens, K.-H. Hong, F. X. Kärtner, and J. Moses, Nat. Photonics **11**, 222 (2017).
15. H. Timmers, A. Kowligy, A. Lind, F. C. Cruz, N. Nader, M. Silfies, G. Ycas, T. K. Allison, P. G. Schunemann, S. B. Papp, and S. A. Diddams, Optica **5**, 727 (2018).
16. S. Vasilyev, I. S. Moskalev, V. O. Smolski, J. M. Peppers, M. Mirov, A. V. Muraviev, K. Zawilski, P. G. Schunemann, S. B. Mirov, K. L. Vodopyanov, and V. P. Gapontsev, Optica **6**, 111 (2019).
17. T. P. Butler, D. Gerz, C. Hofer, J. Xu, C. Gaida, T. Heuermann, M. Gebhardt, L. Vamos, W. Schweinberger, J. A. Gessner, T. Siefke, M. Heusinger, U. Zeitner, A. Apolonski, N. Karpowicz, J. Limpert, F. Krausz, and I. Pupeza, Opt. Lett. **44**, 1730 (2019).
18. G. Ehret, C. Kiemle, M. Wirth, A. Amediek, A. Fix, and S. Houweling, Appl. Phys. B **90**, 593 (2008).
19. H. Bovensmann, J. P. Burrows, M. Buchwitz, J. Frerick, S. Noël, V. V. Rozanov, K. V. Chance, and A. P. H. Goede, J. Atmos. Sci. **56**, 127 (1999).
20. E. Baumann, E. V. Hoenig, E. F. Perez, G. M. Colacion, F. R. Giorgetta, K. C. Cossel, G. Ycas, D. R. Carlson, D. D. Hickstein, K. Srinivasan, S. B. Papp, N. R. Newbury, and I. Coddington, Opt. Express **27**, 11869 (2019).
21. R. Liao, Y. Song, W. Liu, H. Shi, L. Chai, and M. Hu, Opt. Express **26**, 11046 (2018).
22. F. Adler and S. A. Diddams, Opt. Lett. **37**, 1400 (2012).
23. F. Tan, H. Shi, R. Sun, P. Wang, and P. Wang, Opt. Express **24**, 22461 (2016).
24. S. Kumkar, G. Krauss, M. Wunram, D. Fehrenbacher, U. Demirbas, D. Brida, and A. Leitenstorfer, Opt. Lett. **37**, 554 (2012).
25. C. P. Hauri, R. B. Lopez-Martens, C. I. Blaga, K. D. Schultz, J. Cryan, R. Chirla, P. Colosimo, G. Doumy, A. M. March, C. Roedig, E. Sistrunk, J. Tate, J. Wheeler, L. F. DiMauro, and E. P. Power, Opt. Lett. **32**, 868 (2007).
26. B. E. Schmidt, P. Béjot, M. Giguère, A. D. Shiner, C. Trallero-Herrero, É. Bisson, J. Kasparian, J.-P. Wolf, D. M. Villeneuve, J.-C. Kieffer, P. B. Corkum, and F. Légaré, Appl. Phys. Lett. **96**, 121109 (2010).
27. N. Nishizawa and T. Goto, IEEE J. Sel. Top. Quantum Electron. **7**, 518 (2001).
28. P. Ciąćka, A. Rampur, A. Heidt, T. Feurer, and M. Klimczak, J. Opt. Soc. Am. B **35**, 1301 (2018).
29. S. D. Agger and J. H. J. H. Povlsen, Opt. Express **14**, 50 (2006).
30. M. A. Foster, A. L. Gaeta, Q. Cao, and R. Trebino, Opt. Express **13**, 6848 (2005).
31. C. Gaida, T. Heuermann, M. Gebhardt, E. Shestaev, T. P. Butler, D. Gerz, N. Lilienfein, P. Sulzer, M. Fischer, R. Holzwarth, A. Leitenstorfer, I. Pupeza, and J. Limpert, Opt. Lett. **43**, 5178 (2018).
32. C. Gaida, M. Gebhardt, F. Stutzki, C. Jauregui, J. Limpert, and A. Tünnermann, Opt. Lett. **40**, 5160 (2015).
33. J. M. Dudley, G. Genty, and S. Coen, Rev. Mod. Phys. **78**, 1135 (2006).
34. S. Xing, S. Kharitonov, T. North, D. Grassani, and C.-S. Brès, in *Lasers Congress* (2016), paper AM5A.8.
35. S. T. Cundiff and J. Ye, Rev. Mod. Phys. **75**, 325 (2003).
36. T. Qiao, H. Cheng, X. Wen, W. Wang, W. Lin, Y. Zhou, Y. Guo, Y. Liu, and Z. Yang, Opt. Lett. **44**, 6001 (2019).
37. G. Krauss, S. Lohss, T. Hanke, A. Sell, S. Eggert, R. Huber, and A. Leitenstorfer, Nat. Photonics **4**, 33 (2009).